Preparation and Characterization of Homologous Diiron Dithiolato, Diselenato, and Ditellurato Complexes: [FeFe]−Hydrogenase Models

ARTICLE *in* ORGANOMETALLICS · DECEMBER 2009

Impact Factor: 4.13 · DOI: 10.1021/om900675q

ORGANOMETALLICS
Article

Organometallics **XXXX,** *XXX,* 000–000 A
DOI: 10.1021/om900675q

Preparation and Characterization of Homologous Diiron Dithiolato, Diselenato, and Ditellurato Complexes: [FeFe]-Hydrogenase Models

Mohammad K. Harb,[†] Ulf-Peter Apfel,[†] Joachim Kübel,[†] Helmar Görls,[†] Greg A. N. Felton,[‡] Taka Sakamoto,[‡] Dennis H. Evans,*[,‡] Richard S. Glass,*[,‡] Dennis L. Lichtenberger,*[,‡] Mohammad El-khateeb,[§] and Wolfgang Weigand*[,†]

[†]*Institut für Anorganische und Analytische Chemie, Friedrich-Schiller-Universität Jena, August-Bebel-Strasse 2, 07743 Jena, Germany,* [‡]*Department of Chemistry and Biochemistry, The University of Arizona, Tucson, Arizona 85721, and* [§]*Chemistry Department, Jordan University of Science and Technology, 22110 Irbid, Jordan*

Received July 30, 2009

In order to elucidate the influence of the bridging chalcogen atoms in hydrogenase model complexes, diiron dithiolato, diselenolato, and ditellurolato complexes have been prepared and characterized. Treatment of $Fe_3(CO)_{12}$ with 3,3-bis(thiocyanatomethyl)oxetane (**1**) or a mixture of 2-oxa-6,7-dithiaspiro[3.4]octane (**2a**) and 2-oxa-6,7,8-trithiaspiro[3.5]nonane (**2b**) in toluene at reflux afforded the model compound $Fe_2(\mu\text{-}S_2C_5H_8O)(CO)_6$ (**3**). The analogous diselenolato and ditellurolato complexes, $Fe_2(\mu\text{-}Se_2C_5H_8O)(CO)_6$ (**4**) and $Fe_2(\mu\text{-}Te_2C_5H_8O)(CO)_6$ (**5**), were obtained from the reaction of $Fe_3(CO)_{12}$ with 2-oxa-6,7-diselenaspiro[3.4]octane (**6**) and 2-oxa-6,7-ditelluraspiro-[3.4]octane (**7**), respectively. Compounds **3**−**5** were characterized by spectroscopic techniques (NMR, IR, photoelectron spectroscopy), mass spectrometry, single-crystal X-ray analysis, and computational modeling. The electrochemical properties for the new compounds have been studied to assess their ability to catalyze electrochemical reduction of protons to give dihydrogen, and the catalytic rate is found to decrease on going from the sulfur to selenium to tellurium compounds. In the series **3**−**5** the reorganization energy on going to the corresponding cation decreased from **3** to **4** to **5**. Spectroscopic and computational analysis suggests that the increasing size of the chalcogen atoms from S to Se to Te increases the Fe−Fe distance and decreases the ability of the complex to form the structure with a rotated $Fe(CO)_3$ group that has a bridging carbonyl ligand and a vacant coordination site for protonation. This effect is mirrored on reduction of **3**−**5** in that the rotated structure with a bridging carbonyl, which creates a vacant coordination site for protonation, is disfavored on going from the S to Se to Te complexes.

Introduction

The natural energy resources predominantly used today are diminishing, and their continued use has become more harmful for the environment. Therefore, efforts to develop alternative energy resources and fuels have become major goals for the scientific community. Dihydrogen is one of the future fuels that causes no deleterious products for the environment.[1−5] Efficient production of dihydrogen in good yield has become a challenge, and there has been much research aimed at overcoming this challenge.[6−12] Biomimetic catalysts, shown in Scheme 1a,[13−29] are based on the active site of [FeFe]-hydrogenases[5,30−34] (the identity of X in the enzyme is still unclear).[34−41] Recently, diiron complexes containing diselenolato ligands have been prepared and

*Corresponding authors. E-mail: dhevans@email.arizona.edu; rglass@u.arizona.edu; dlichten@email.arizona.edu; c8wewo@uni-jena.de.

(1) Melis, A.; Zhang, L.; Forestier, M.; Ghirardi, M. L.; Seibert, M. *Plant Physiol.* **2000**, *122*, 127.
(2) Cammack, R.; Frey, M.; Robson, R. *Hydrogen as a Fuel: Learning from Nature*; Taylor & Francis: London, 2001.
(3) Woodward, J.; Orr, M.; Cordray, K.; Greenbaum, E. *Nature* **2000**, *405*, 1014.
(4) Coontz, R.; Hanson, B. *Science* **2004**, *305*, 957.
(5) Shima, S.; Pilak, O.; Vogt, S.; Schick, M.; Stagni, M. S.; Meyer-Klaucke, W.; Warkentin, E.; Thauer, R. K.; Ermler, U. *Science* **2008**, *321*, 572.
(6) Zhang, Y. H. P.; Evans, B. R.; Mielenz, J. R.; Hopkins, R. C.; Adams, M. W. W. *PLoS ONE* **2007**, *2*, e456.
(7) Antal, M. J.; Allen, S. G.; Schulman, D.; Xu, X.; Divilio, R. J. *Ind. Eng. Chem. Res.* **2000**, *39*, 4040.
(8) Hallenbeck, P. C.; Benemann, J. R. *Int. J. Hydrogen Energy* **2002**, *27*, 1185.
(9) Cortright, R. D.; Davda, R. R.; Dumesic, J. A. *Nature* **2002**, *418*, 964.
(10) Huber, G. W.; Shabaker, J. W.; Dumesic, J. A. *Science* **2003**, *300*, 2075.
(11) Deluga, G. A.; Salge, J. R.; Schmidt, L. D.; Verykios, X. E. *Science* **2004**, *303*, 993.
(12) Adams, M. W. W.; Stiefel, E. I. *Science* **1998**, *282*, 1842.
(13) Zhao, X.; Georgakaki, I. P.; Miller, M. L.; Yarbrough, J. C.; Darensbourg, M. Y. *J. Am. Chem. Soc.* **2001**, *123*, 9710.
(14) Zhao, X.; Chiang, C.; Miller, M. L.; Rampersad, M. V.; Darensbourg, M. Y. *J. Am. Chem. Soc.* **2003**, *125*, 518.
(15) Gloaguen, F.; Lawrence, J. D.; Rauchfuss, T. B. *J. Am. Chem. Soc.* **2001**, *123*, 9476.
(16) Lyon, E. J.; Georgakaki, I. P.; Reibenspies, J. H.; Darensbourg, M. Y. *J. Am. Chem. Soc.* **2001**, *123*, 3268.

Scheme 1

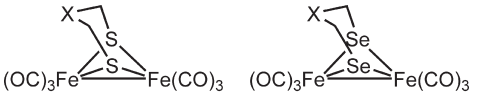

a) X = CH_2, O, NH, S b) X = NPh, CH_2, Se, CHO(Sugar)

characterized (Scheme 1b), and their ability to catalyze H_2 production from acids was evaluated.[42−45]

Photoelectron spectroscopy and theoretical calculations revealed that the reorganization energy of $Fe_2(\mu\text{-}Se_2\text{-}C_3H_5CH_3)(CO)_6$ is substantially lower than that for analogous complexes with Fe_2S_2 cores.[44] This effect, which may lead to faster electron transfer with complexes containing Fe_2Se_2 rather than Fe_2S_2 cores, has not yet been investigated in detail. On the basis of these observations, we have now extended our studies also to the preparation of complexes containing ditellurolato ligands. In the present publication, the preparation of oxetane-containing dithiolato, diselenolato, and ditellurolato diiron complexes is reported (Scheme 2). The ability of these complexes to catalyze the formation of molecular hydrogen from weak acids is presented and compared with related systems. To compare S, Se, and Te analogues, it is important to have the same substitution pattern except for the chalcogen in each complex. This was achieved by synthesizing the homologous series **3**−**5** shown in Scheme 2. The oxetane ring allows the five-membered ring to which it is attached to be stable for all three 1,2-dichalcogenolanes. These precursors to the desired complexes do not polymerize, as is readily seen with the unsubstituted compounds.

Scheme 2

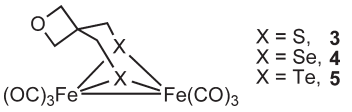

Experimental Section

General Comments. All reactions were carried out under an argon atmosphere with standard Schlenk techniques. THF, toluene, and hexane were dried and distilled prior to use according to standard methods. The ^1H, $^{13}C\{^1H\}$, $^{77}Se\{^1H\}$, and 2D NMR (^1H,^1H COSY, ^1H,^{13}C HSQC, ^1H,^{77}Se HMBC) spectra were recorded on either a Bruker AVANCE 200 or 400 MHz spectrometer using the solvent residual peak or a concentrated solution of SeO_2 in D_2O as reference. The ^{77}Se chemical shifts are reported relative to neat Me_2Se [$\delta(Me_2Se) = \delta(SeO_2) + 1302.6$ ppm].[46] The ^{125}Te chemical shift was measured versus external PhTeTePh and converted to that versus Me_2Te.[47] Mass spectra were recorded on a Finnigan MAT SSQ 710 instrument. IR spectra were measured as KBr disks on a Perkin-Elmer System 2000 FT-IR spectrometer and in Nujol on a Thermo Nicolet Avatar ESP 380 FT-IR spectrometer utilizing the OMNIC version 6.1 software. Elemental analyses were performed with a LECO CHNS-932 apparatus. Silica gel 60 (0.015−0.040 mm) was used for column chromatography, and TLC was done using Merck TLC aluminum sheets (silica gel 60 F254). 3,3-Bis(thiocyanatomethyl)oxetane[48] (**1**), a 2-oxa-6,7-dithiaspiro[3.4]octane (**2a**) and 2-oxa-6,7,8-trithiaspiro[3.5]-nonane (**2b**) mixture,[48] 2-oxa-6,7-disellenaspiro[3.4]octane[49] (**6**), and 2-oxa-6,7-ditelluraspiro[3.4]octane[50] (**7**) were prepared according to literature protocols. $Fe_3(CO)_{12}$ purchased from Aldrich, solvents from Fisher Scientific, and other chemicals from Acros were used without further purification. Yield calculations were based on substoichiometric utilized chemicals or on $Fe_3(CO)_{12}$ for the diiron complexes.

Synthesis of $Fe_2(\mu\text{-}S_2C_5H_8O)(CO)_6$ (3). Method A. A solution of $Fe_3(CO)_{12}$ (140 mg, 0.28 mmol) and **1** (56 mg, 0.28 mmol) in toluene (25 mL) was heated under reflux for one hour. The resulting dark red mixture was evaporated to dryness under reduced pressure. The obtained solid was redissolved in a

(17) Lawrence, J. D.; Li, H.; Rauchfuss, T. B.; Benard, M.; Rohmer, M. *Angew. Chem., Int. Ed.* **2001**, *40*, 1768.
(18) Razavet, M.; Davies, S. C.; Hughes, D. L.; Barclay, J. E.; Evans, D. J.; Fairhurst, S. A.; Liu, X.; Pickett, C. J. *J. Chem. Soc., Dalton Trans.* **2003**, 586.
(19) Linck, R. C.; Rauchfuss, T. B. In *Synthetic models for bioorganometallic reaction centers*; Bioorganometallics; Wiley-VCH Verlag GmbH & Co.: Weinheim, Germany, 2006; p 403.
(20) Li, H.; Rauchfuss, T. B. *J. Am. Chem. Soc.* **2002**, *124*, 726.
(21) Tard, C.; Liu, X.; Ibrahim, S. K.; Bruschi, M.; De Gioia, L.; Davies, S. C.; Yang, X.; Wang, L.; Sawers, G.; Pickett, C. J. *Nature* **2005**, *433*, 610.
(22) Song, L.-C.; Yang, Z. Y.; Bian, H. Z.; Hu, Q. M. *Organometallics* **2004**, *23*, 3082.
(23) Seyferth, D.; Henderson, R. S.; Song, L.-C. *Organometallics* **1982**, *1*, 125.
(24) Windhager, J.; Rudolph, M.; Bräutigam, S.; Görls, H.; Weigand, W. *Eur. J. Inorg. Chem.* **2007**, 2748.
(25) Windhager, J.; Goerls, H.; Petzold, H.; Mloston, G.; Linti, G.; Weigand, W. *Eur. J. Inorg. Chem.* **2007**, 4462.
(26) Song, L.-C.; Yang, Z. Y.; Bian, H. Z.; Liu, Y.; Wang, H. T.; Liu, X. F.; Hu, Q. M. *Organometallics* **2005**, *24*, 6126.
(27) Tard, C.; Pickett, C. *J. Chem. Rev.* **2009**, *109*, 2245.
(28) Windhager, J.; Seidel, R. A.; Apfel, U.; Görls, H.; Linti, G.; Weigand, W. *Chem. Biodiversity* **2008**, *5*, 2023.
(29) Ott, S.; Kritikos, M.; Åkermark, B.; Sun, L. *Angew. Chem., Int. Ed.* **2003**, *42*, 3285.
(30) Albracht, S. P. J. *Biochim. Biophys. Acta, Bioenerg.* **1994**, *1188*, 167.
(31) Graf, E.; Thauer, R. K. *FEBS Lett.* **1981**, *136*, 165.
(32) Cammack, R.; Patil, D.; Aguirre, R.; Hatchikian, E. C. *FEBS Lett.* **1982**, *142*, 289.
(33) Wang, G.; Benecky, M.; Huynh, B.; Cline, J.; Adams, M.; Mortenson, L.; Hoffman, B.; Munck, E. *J. Biol. Chem.* **1984**, *259*, 14328.
(34) Adams, M. W.; Mortenson, L. E. *J. Biol. Chem.* **1984**, *259*, 7045.
(35) Chen, J.; Mortenson, L. E. *Biochim. Biophys. Acta, Protein Struct.* **1974**, *371*, 283.
(36) Chen, J.; Blanchard, D. K. *Biochem. Biophys. Res. Commun.* **1978**, *84*, 1144.
(37) Glick, B. R.; Martin, W. G.; Martin, S. M. *Can. J. Microbiol.* **1980**, *26*, 1214.
(38) Adams, M. W. W.; Mortenson, L. E. *Biochim. Biophys. Acta, Bioenerg.* **1984**, *766*, 51.
(39) Fauque, G.; Peck, H. D.Jr.; Moura, J. J. G.; Huynh, B. H.; Berlier, Y.; DerVartanian, D. V.; Teixeira, M.; Przybyla, A. E.; Lespinat, P. A. *FEMS Microbiol. Rev.* **1988**, *54*, 299.
(40) Adams, M. W. *Biochim. Biophys. Acta* **1990**, *1020*, 115.
(41) Hatchikian, E. C.; Forget, N.; Fernandez, V. M.; Williams, R.; Cammack, R. *Eur. J. Biochem.* **1992**, *209*, 357.
(42) Gao, S.; Fan, J.; Sun, S.; Peng, X.; Zhao, X.; Hou, J. *Dalton Trans.* **2008**, 2128.
(43) (a) Song, L.-C.; Gai, B.; Wang, H.; Hu, Q. *J. Inorg. Biochem.* **2009**, *103*, 805. (b) Song, L.-C.; Gao, W.; Feng, C.-P.; Wang, D.-F.; Hu, Q.-M. *Organometallics* **2009**, *28*, 6121.
(44) Harb, M. K.; Niksch, T.; Windhager, J.; Görls, H.; Holze, R.; Lockett, L. T.; Okumura, N.; Evans, D. H.; Glass, R. S.; Lichtenberger, D. L.; El-khateeb, M.; Weigand, W. *Organometallics* **2009**, *28*, 1039.
(45) Apfel, U.; Halpin, Y.; Gottschaldt, M.; Görls, H.; Vos, J. G.; Weigand, W. *Eur. J. Inorg. Chem.* **2008**, *2008*, 5112.
(46) Burns, R. C.; Collins, M. J.; Gillespie, R. J.; Schrobilgen, G. J. *Inorg. Chem.* **1986**, *25*, 4465.
(47) Granger, P.; Chapelle, S.; McWhinnie, W. R.; Al-Rubaie, A. *J. Organomet. Chem.* **1981**, *220*, 149.
(48) Campbell, T. W. *J. Org. Chem.* **1957**, *22*, 1029.
(49) Günther, W. H.; Salzman, M. N. *Ann. N.Y. Acad. Sci.* **1972**, *192*, 25.
(50) Lakshmikantham, M. V.; Cava, M. P.; Gunther, W. H. H.; Nugara, P. N.; Belmore, K. A.; Atwood, J. L.; Craig, P. *J. Am. Chem. Soc.* **1993**, *115*, 885.

minimum amount of CH_2Cl_2 and column chromatographed. From the major red fraction, which was eluted with THF/hexane (1:3), **3** was obtained as a red solid (56 mg, 47%).

Method B. Twenty-five milligrams of the 2-oxa-6,7-dithiaspiro[3.4]octane and 2-oxa-6,7,8-trithiaspiro[3.5]nonane mixture (**2a** and **2b**) and $Fe_3(CO)_{12}$ (85 mg, 0.169 mmol) were dissolved in 20 mL of toluene and heated under reflux for 1.5 h. Evaporation and column chromatography (THF/hexane, 1:3) gave 36 mg (50%) of the red crystalline product **3**. Anal. Calcd for $C_{11}H_8Fe_2O_7S_2 \cdot 1$hexane: C, 32.34; H, 2.29, S, 14.56. Found: C, 32.27; H, 2.31, S, 14.16. IR $\nu_{C\equiv O}$ cm^{-1}: (KBr disk) 2076 (vs), 2033 (vs), 1997 (vs, sh), (Nujol) 2077 (s), 2036 (vs), 2008 (s), 1993 (s), 1982 (m). ^1H NMR (200 MHz, $CDCl_3$): δ 4.28 (s, 4H, $(CH_2)_2O$), 2.48 (s, 4H, $2SCH_2$). ^1H NMR (200 MHz, −50 °C, $CDCl_3$): δ 4.28 (s, 4H, $(CH_2)_2O$), 3.07 (d, $^2J_{H,H}$ = 8.8 Hz, 2H, SCH_AH_B and SCH_CH_D), 1.81 (d, $^2J_{H,H}$ = 8.8 Hz, 2H, SCH_AH_B and SCH_CH_D). ^{13}C NMR (50 MHz, $CDCl_3$): δ 207.1 (CO), 82.2 ($(CH_2)_2O$), 42.2 (C_q), 30.3 ($2SCH_2$). DEI-MS (m/z): 428 (M^+), 400 ($M^+ - CO$), 372 ($M^+ - 2CO$), 344 ($M^+ - 3CO$), 316 ($M^+ - 4CO$), 288 ($M^+ - 5CO$), 260 ($M^+ - 6CO$).

Synthesis of $Fe_2(\mu\text{-}Se_2C_5H_8O)(CO)_6$ (4). A solution of $Fe_3(CO)_{12}$ (101 mg, 0.2 mmol) and **5** (49 mg, 0.2 mmol) in THF (50 mL) was heated at reflux for one hour. The resulting mixture was evaporated to dryness in vacuo. The obtained solid was suspended in a minimum amount of hexane and chromatographed on silica gel, eluting with CH_2Cl_2/hexane (1:3). From the major red fraction, **4** was obtained as a red solid (73 mg, 70%). Single crystals were obtained from hexane solution. Mp: 169−170 °C. Anal. Calcd for $C_{11}H_8Fe_2O_7Se_2$: C, 25.32; H, 1.55. Found: C, 25.14; H, 1.66. IR $\nu_{C\equiv O}$ cm^{-1}: (KBr disk) 2068 (vs), 2025 (vs), 1988 (vs) cm^{-1}, (Nujol) 2070 (s), 2029 (vs), 2000 (s), 1989 (s), 1977 (m). ^1H NMR (200 MHz, $CDCl_3$): δ 4.26 (s, 4H, $(CH_2)_2O$), 2.52 (s, 4H, 2SeCH2). ^1H NMR (200 MHz, −50 °C, $CDCl_3$): δ 4.26 (s, 4H, $(CH_2)_2O$), 3.15 (d, $^2J_{H,H}$ = 10.2 Hz, 2H, $SeCH_AH_B$ and $SeCH_CH_D$), 1.89 (d, $^2J_{H,H}$ = 10.2 Hz, 2H, $SeCH_AH_B$ and $SeCH_CH_D$). ^{13}C NMR (50 MHz, $CDCl_3$): δ 208.2 (CO), 81.8 ($(CH_2)_2O$), 42.2 (C_q), 21.5 ($2SeCH_2$). $^{77}Se\{^1H\}$ NMR (76 MHz, $CDCl_3$): δ 107 ppm. DEI-MS (m/z): 524 (M^+), 496 ($M^+ - CO$), 468 ($M^+ - 2CO$), 440 ($M^+ - 3CO$), 411 ($M^+ - 4CO$), 384 ($M^+ - 5CO$), 356 ($M^+ - 6CO$).

Synthesis of $Fe_2(\mu\text{-}Te_2C_5H_8O)(CO)_6$ (5). Complex **5** was prepared, separated, and recrystallized by a procedure similar to that of **4**. The reaction of $Fe_3(CO)_{12}$ (101 mg, 0.2 mmol) with **6** (68 mg, 0.2 mmol) was carried out in THF. Yield: 82 mg (66%). Mp: 175−176 °C. Anal. Calcd for $C_{11}H_8Fe_2O_7Te_2 \cdot 0.25$hexane: C, 23.44; H, 1.81. Found: C, 23.24; H, 1.99. IR $\nu_{C\equiv O}$ cm^{-1}: (KBr disk) 2055 (s), 2012 (vs), 1971 (vs) cm^{-1}, (Nujol) 2058 (s), 2020 (vs), 1990 (s), 1982 (s), 1969 (m). ^1H NMR (200 MHz, $CDCl_3$): δ 4.23 (s, 4H, $(CH_2)_2O$), 2.66 (s, 4H, $2TeCH_2$). ^1H NMR (200 MHz, −50 °C, $CDCl_3$): δ 4.48 (s, 2H, $CH_{2A}O$), 4.04 (s, 2H, $CH_{2B}O$) 3.22 (s, 2H, $TeCH_AH_B$ and $TeCH_CH_D$), 2.12 (s, 2H, $TeCH_AH_B$ and $TeCH_CH_D$). ^{13}C NMR (50 MHz, $CDCl_3$): δ 210 (CO), 80.2 ($(CH_2)_2O$), 42.3 (C_q), 4.2 ($2TeCH_2$). ^{125}Te NMR (158 MHz, $CDCl_3$): δ 197. DEI-MS (m/z): 620 (M^+), 496, 564 ($M^+ - 2CO$), 508 ($M^+ - 4CO$), 452 ($M^+ - 6CO$).

Crystal Structure Determination. The intensity data for the compounds were collected on a Nonius KappaCCD diffractometer, using graphite-monochromated Mo Kα radiation. Data were corrected for Lorentz and polarization effects, but not for absorption effects.[51,52] The structures were solved by direct methods (SHELXS)[53] and refined by full-matrix least-squares techniques against F_o^2 (SHELXL-97).[54] All hydrogen atoms were included at calculated positions with fixed thermal parameters. All non-hydrogen atoms were refined anisotropically. XP (SIEMENS Analytical X-ray Instruments, Inc.) was used for structure representations.

Electrochemical Measurements. Instrumentation and the source and treatment of solvent and supporting electrolyte have been reported earlier.[55] All potentials are reported versus the potential of the ferrocenium/ferrocene (Fc^+/Fc) couple measured in acetonitrile. The voltammetric experiments were conducted at 298 K, using ∼1.0 mM of each compound in acetonitrile containing 0.10 M Bu_4NPF_6 on a glassy carbon working electrode (GCE), under an Ar atmosphere. The area of the GCE was determined to be 0.0707 cm^2 from cyclic voltammetric studies of the oxidation of ferrocene in acetonitrile using 2.5×10^{-5} cm^2/s as its diffusion coefficient.[55]

Photoelectron Spectroscopy. Photoelectron spectra were recorded using an instrument that features a 36 cm radius hemispherical analyzer (McPherson),[56] with custom-designed photon source, sample cells, detection and control electronics, calibration, and data analysis as described previously.[57] In the figures of the photoelectron spectra, the spectra obtained with the He I source photons are represented by the solid black lines, and the spectra obtained with the He II source photons are represented with the red dashed lines. The He II spectra are scaled to match the low ionization energy intensities in the He I spectra for visual comparison of the change in relative intensity at higher ionization energies. All samples sublimed cleanly, with no visible changes in the spectra during data collection after initial observation of ionizations from the diiron complex. The sublimation temperatures for the compounds (in °C, at 10^{-5} Torr) were as follows: complex **3**, 90−110; **4**, 100−110; **5**, 110−120.

Density Functional Theory (DFT) Calculations. Computational methods have been developed previously for this class of diiron hexacarbonyl systems with S and Se heteroatoms in the bridging positions and validated by their ability to account for structures, adiabatic ionization energies, carbonyl stretching frequencies, pK_a values, oxidation and reduction potentials, and other electrochemical parameters, as well as metal−metal and pertinent metal−ligand bond energies.[44,58−60] Density functional theory calculations were carried out with the Amsterdam density functional (ADF2006.01d) package.[61,62] Geometry optimizations and frequency calculations (with no imaginary frequencies in the final geometries) were carried out using the VWN functional with the Stoll correction implemented.[63] All electronic energies were obtained with the OPBE functional.[64] Comparison of the OPBE functional to other common functionals found it to be the best for the prediction of nuclear

(51) Nonius, B. V. *COLLECT, Data Collection Software*, **1998**.
(52) Otwinowski, Z.; Minor, W. In *Processing of X-ray diffraction data collected in oscillation mode*; Carter, C. W., Jr., Ed.; Methods in Enzymology; Academic Press: New York, 1997; Vol. *276*, pp 307−326.
(53) Sheldrick, G. M. *Acta Crystallogr., Sect. A* **1990**, *46*, 467.
(54) Sheldrick,G. M. *SHELXL-97* (*Release 97-2*); **1997**.
(55) Macías-Ruvalcaba, N. A.; Evans, D. H. *J. Phys. Chem. B* **2005**, *109*, 14642.
(56) Siegbahn, K.; Nordling, C.; Fahlman, A.; Nordberg, R.; Hamrin, K.; Hedman, J.; Johansson, G.; Bergmark, T.; Karlsson, S. E.; Lindgren, I.; Lindberg, B. *Nova Acta Regiae Societatis Scientiarum Upsaliensis* **1967**, *20*, 282.
(57) Cranswick, M. A.; Dawson, A.; Cooney, J. J. A.; Gruhn, N. E.; Lichtenberger, D. L.; Enemark, J. H. *Inorg. Chem.* **2007**, *46*, 10639.
(58) Felton, G. A. N.; Vannucci, A. K.; Chen, J.; Lockett, L. T.; Okumura, N.; Petro, B. J.; Zakai, U. I.; Evans, D. H.; Glass, R. S.; Lichtenberger, D. L. *J. Am. Chem. Soc.* **2007**, *129*, 12521.
(59) Petro, B. J.; Vannucci, A. K.; Lockett, L. T.; Mebi, C.; Kottani, R.; Gruhn, N. E.; Nichol, G. S.; Goodyer, P. A. J.; Evans, D. H.; Glass, R. S.; Lichtenberger, D. L. *J. Mol. Struct.* **2008**, *890*, 281.
(60) Felton, G. A. N.; Vannucci, A. K.; Okumura, N.; Lockett, L. T.; Evans, D. H.; Glass, R. S.; Lichtenberger, D. L. *Organometallics* **2008**, *27*, 4671.
(61) Te Velde, G.; Bickelhaupt, F. M.; Baerends, E. J.; Fonseca Guerra, C.; Van Gisbergen, S. J. A.; Snijders, J. G.; Ziegler, T. *J. Comput. Chem.* **2001**, *22*, 931.
(62) *ADF2006.01d, SCM*, Theoretical Chemistry, Vrije Universiteit: Amsterdam, The Netherlands, 2006.
(63) Stoll, H.; Pavlidou, C. M. E.; Preuss, H. *Theor. Chim. Acta* **1978**, *49*, 143.
(64) Swart, M.; Ehlers, A. W.; Lammertsma, K. *Mol. Phys.* **2004**, *102*, 2467.

Scheme 3

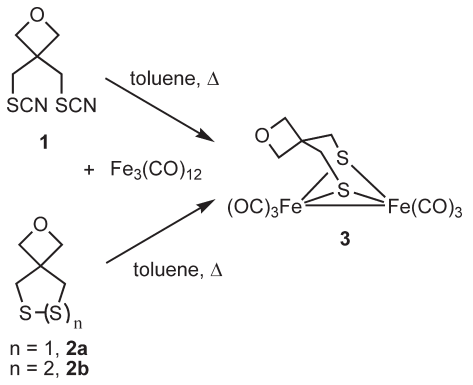

Scheme 4

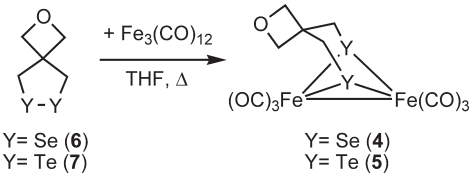

magnetic constants[65] and the only functional to correctly predict the spin states of seven different iron complexes.[64] All calculations utilized a triple-ζ Slater-type orbital (STO) basis set with one polarization function (TZP) for H, C, O, Fe, S, and Se and two polarization functions (TZ2P) for Te. Relativistic effects by the zero-order regular approximation (ZORA)[66,67] were also applied during all calculations. The frozen core approximation was used for the inner core of all atoms. The theoretical stretching frequencies and IR absorption intensities for all species were calculated analytically with the same computing method as described above and scaled by a factor of 1.002. For the simulated IR spectra in the figure the linewidths are adjusted by a constant factor to approximate the linewidths in the experimental spectra. Figures of the optimized geometries and molecular orbital plots were created with Molekel.[68]

Results and Discussion

Treatment of $Fe_3(CO)_{12}$ with bisthiocyanate **1** in toluene under reflux for one hour afforded the diiron dithiolato complex $Fe_2(\mu\text{-}S_2C_5H_8O)(CO)_6$ (**3**). Moreover, complex **3** also was prepared from the reaction of $Fe_3(CO)_{12}$ with an inseparable 1:1 mixture of **2a** and **2b**[48] in toluene under reflux conditions for one and a half hour in 50% yield (Scheme 3).

The analogous diselenolato and ditellurolato complexes $Fe_2(\mu\text{-}Se_2C_5H_8O)(CO)_6$ (**4**) and $Fe_2(\mu\text{-}Te_2C_5H_8O)(CO)_6$ (**5**) were synthesized from the reaction of $Fe_3(CO)_{12}$ with 2-oxa-6,7-diselenaspiro[3.4]octane (**6**) or 2-oxa-6,7-ditelluraspiro-[3.4]octane (**7**), respectively. These reactions were carried out in THF (Scheme 4).

Compounds **3**−**5** are air-stable in the solid state and for several hours in solution. These products were characterized by IR spectroscopy, multinuclear NMR spectroscopy, mass spectrometry, elemental analysis, X-ray crystallography, and photoelectron spectroscopy.

The room-temperature ^{1}H NMR spectra of **3**−**5** display two singlets at 2.48 and 4.28 (**3**), 2.52 and 4.26 (**4**), and 2.66 and 4.23 (**5**) ppm for the two different methylene groups YCH_2 (Y = S, Se, Te) and CH_2O, respectively. Upon cooling to −50 °C, the resonance signals of the more shielded methylene groups in **3** and **4** split into AB spin systems, since ring flipping of the three-carbon bridge is frozen out and the hydrogen atoms of YCH_2 (Y = S, Se) are now nonequivalent. The low-temperature (−50 °C) ^{1}H NMR spectrum of **5** displays two unresolved signals of an AB spin system corresponding to the diastereotopic protons at $TeCH_2$, as well as two broad singlets for the CH_2OCH_2 group. The $^{13}C\{^1H\}$ NMR spectra of **3**−**5** exhibit three resonances at 82.2, 42.2, and 30.3 (**3**), 81.8, 42.2, and 21.5 (**4**), and 80.2, 42.3, and 4.2 (**5**) for CH_2O, C_q, and YCH_2 (Y = S, Se, Te). The ^{13}C resonance of $TeCH_2$ in **5** is significantly shifted to high field ($\Delta\delta$(S,Te) = 26.1, $\Delta\delta$(Se,Te) = 17.3), which could be attributed to the "heavy atom" effect.[69] One signal is observed at 107 ppm in the ^{1}H,^{77}Se HMBC NMR spectrum of **4**, indicating equivalent Se atoms. This resonance is shifted to higher field compared to that of the propanediselenolato (PDS) model complex (145 ppm).[43,44] The mass spectra of **3**−**5** showed the molecular ion peaks and the elimination of six CO ligands sequentially.

The IR spectra of complexes **3**−**5** (KBr disk) exhibit three strong absorption bands in the regions 1997−2076 for **3**, 1988−2068 for **4**, and 1971−2055 cm^{-1} for **5**. When comparing the spectra, it can be seen that the CO absorption bands are shifted to lower frequencies from **3** to **5**, which can be explained by the increasing back-donation to CO caused by rising donor ability from S to Te. These data are within the same ranges as those observed for propanedithiolato (PDT),[70] PDS,[43,44] and propaneditellurolato (PDTe)[71] complexes.

The X-ray diffraction analyses reveal the proposed structures of **3**−**5** as shown in Figures 1−3 and Table 1. The central 2Fe2Y (Y = S, Se, Te) moieties of **3**−**5** are in the butterfly conformation and the geometry around the iron atoms is similar to that reported for PDT, PDS, and PDTe complexes.[43,44,70,71] The Fe−Fe bond distances in **3**−**5** are 2.4923(3), 2.5367(19), and 2.6322(11) Å, respectively, a trend attributed to the increase of atomic sizes from S to Te. The Fe−S, Fe−Se, and Fe−Te bond lengths are comparable to those reported for PDT, PDS, and PDTe complexes.[43,44,70,71] Moreover an increase of the bonding angle X−C1−C2 (X = S, Se, Te) is visible (**3**: 117.76(12)°, **4**: 118.2(6)°, **5**: 118.5(4)°). These values are unexpectedly high in comparison to a regular sp^3-hybridized atom (109.5°). An explanation for this is given in the literature and can be described by the rule of Bent.[72,73]

It is noteworthy that the Fe−CO bond lengths {average lengths: 1.800 Å (**3**), 1.793 Å (**4**), 1.785 Å (**5**)} are slightly decreasing from **3** to **5** due to the increasing electron density at the Fe atoms caused by more back-donation ability from S

(65) Zhang, Y.; Lin, H.; Truhlar, D. G. *J. Chem. Theory Comput.* **2007**, *3*, 1378.
(66) van Lenthe, E.; Ehlers, A.; Baerends, E. *J. Chem. Phys.* **1999**, *110*, 8943.
(67) van Lenthe, E.; Baerends, E. J.; Snijders, J. G. *J. Chem. Phys.* **1993**, *99*, 4597.
(68) Portmann, S.; Luthi, H. P. *Chimia* **2000**, *54*, 766.
(69) Kalabin, G. A.; Bzhezovskii, V. M.; Kushnarev, D. F.; Proidakov, A. G. *Zh. Org. Khim* **1981**, *17*, 1143.
(70) Lyon, E. J.; Georgakaki, I. P.; Rabenspies, J. H.; Darensbourg, M. Y. *Angew. Chem., Int. Ed.* **1999**, *38*, 3178.
(71) Shieh, M.; Shieh, M. H. *Organometallics* **1994**, *13*, 920.
(72) Apfel, U.; Halpin, Y.; Görls, H.; Vos, J. G.; Schweizer, B.; Linti, G.; Weigand, W. *Chem. Biodiversity* **2007**, *4*, 2138.
(73) Bent, H. A. *Chem. Rev.* **1961**, *61*, 275.

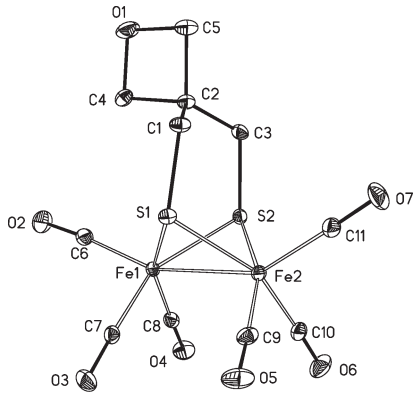

Figure 1. ORTEP drawing of $Fe_2(\mu\text{-}S_2C_5H_8O)(CO)_6$ (**3**) with thermal ellipsoids set at the 50% probability level (hydrogen atoms were omitted for clarity). Selected distances [Å] and angles [deg]: Fe1−Fe2 2.4923(3), Fe1−S1 2.2682(5), Fe1−S2 2.2676(5), Fe2−S1 2.2578(5), Fe2−S2 2.2600(5), Fe1−S1−Fe2 66.826(14), Fe1−S2−Fe2 66.799(14), S1−Fe1−S2 84.279(17), S1−Fe2−S2 84.690(17).

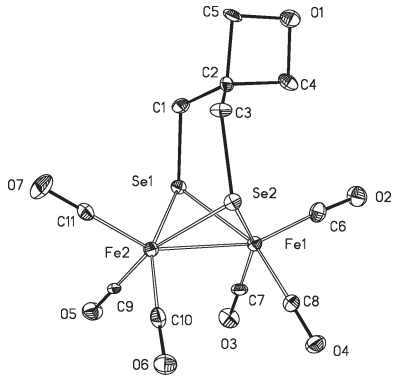

Figure 2. ORTEP drawing of $Fe_2(\mu\text{-}Se_2C_5H_8O)(CO)_6$ (**4**) with thermal ellipsoids set at the 50% probability level (hydrogen atoms were omitted for clarity). Selected distances [Å] and angles [deg]: Fe1−Fe2 2.5367(19), Fe1−Se1 2.3813(15), Fe1−Se2 2.3824(14), Fe2−Se1 2.3753(16), Fe2−Se2 2.3823(17), Fe1−Se1−Fe2 64.46(5), Fe1−Se2−Fe2 64.34(5), Se1−Fe1−Se2 85.61(5), Se1−Fe2−Se2 85.74(6).

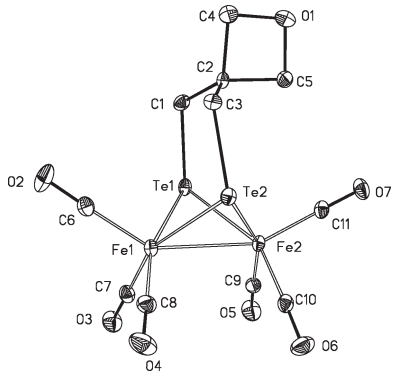

Figure 3. ORTEP drawing of $Fe_2(\mu\text{-}Te_2C_5H_8O)(CO)_6$ (**5**) with thermal ellipsoids set at the 50% probability level (hydrogen atoms were omitted for clarity). Selected distances [Å] and angles [deg]: Fe1−Fe2 2.6322(11), Fe1−Te1 2.5435(8), Fe1−Te2 2.5344(8), Fe2−Te1 2.5317(8), Fe2−Te2 2.5384(7), Fe1−Te1−Fe2 62.48(3), Fe1−Te2−Fe2 62.52(2), Te1−Fe1−Te2 86.92(3), Te1−Fe2−Te2 87.09(2).

Table 1. Crystal Data and Refinement Details for the X-Ray Structure Determinations of the Compounds 3, 4, and 5

	3	**4**	**5**
formula	$C_{11}H_8Fe_2O_7S_2$	$C_{11}H_8Fe_2O_7Se_2$	$C_{11}H_8Fe_2O_7Te_2$
fw	427.99	521.79	619.07
T/°C	−90(2)	−90(2)	−90(2)
cryst syst	triclinic	triclinic	triclinic
space group	$P\bar{1}$	$P\bar{1}$	$P\bar{1}$
a/Å	8.7511(3)	8.7942(7)	7.7877(4)
b/Å	9.3583(4)	9.4877(11)	9.0734(4)
c/Å	10.2267(3)	10.3124(13)	12.6096(6)
α/deg	100.509(2)	100.635(7)	101.493(2)
β/deg	91.881(2)	92.451(7)	95.493(2)
γ/deg	110.795(2)	110.565(7)	110.171(3)
V/Å^3	765.48(5)	786.33(15)	806.39(7)
Z	2	2	2
ρ/g·cm^{-3}	1.857	2.204	2.550
μ/cm^{-1}	21.95	65.01	53.72
measd data	5538	5339	5678
data with $I > 2\sigma(I)$	3198	1946	2893
unique data/R_{int}	3484/0.0231	3540/0.0868	3644/0.0364
wR_2 (all data, on F^2)[a]	0.0636	0.1352	0.0860
R_1 ($I > 2\sigma(I)$)[a]	0.0246	0.0655	0.0378
s[b]	1.021	1.004	1.046
res dens/e·Å^{-3}	0.420/−0.414	0.989/−1.183	0.785/−1.366
absorpt method	none	none	none
CCDC no.	723576	723577	723578

[a] $R_1 = (\sum||F_o|-|F_c||)/\sum|F_o|$, $wR_2 = \{\sum[w(F_o^2 - F_c^2)^2]/\sum[w(F_o^2)^2]\}^{1/2}$ with $w^{-1} = \sigma^2(F_o^2) + (\alpha P)^2$. [b] $s = \{\sum[w(F_o^2 - F_c^2)^2]/(N_o - N_p)\}^{1/2}$.

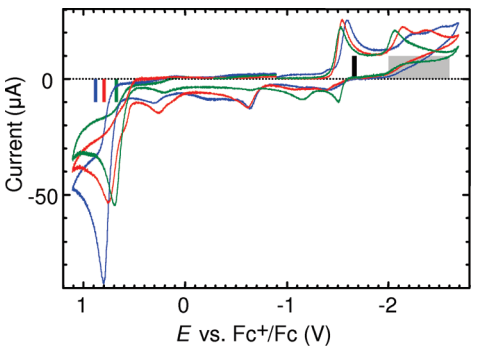

Figure 4. Background-corrected voltammograms of 1.01 mM **3** (blue), 1.00 mM **4** (red), and 1.00 mM **5** (green) in acetonitrile with 0.10 M tetrabutylammonium hexafluorophosphate at glassy carbon (0.10 V/s; scan segments: −0.9 to −2.7 V; −2.7 to +1.1 V; +1.1 to −0.9 V; argon purged). The bars on the zero current axis represent the oxidation and reduction potentials obtained from DFT computations. The colored bars are the calculated oxidation potentials for each respective molecule, the black bar is the range of calculated first reduction potentials for all three molecules, and the gray bar represents the range of calculated second reduction potentials for a variety of final geometries.

to Te. This observation is consistent with the CO band shifts to lower frequencies from **3** to **5** in their IR spectra.

Electrochemical Investigations. Cyclic voltammograms (CV) of **3**−**5** were recorded in order to observe the electrochemically induced reduction and oxidation properties of this family of compounds and to assess their ability to catalyze the reduction of weak acids to form dihydrogen. Comparison of a wide potential range of CV data, Figure 4, for all three compounds shows some broadly similar processes.

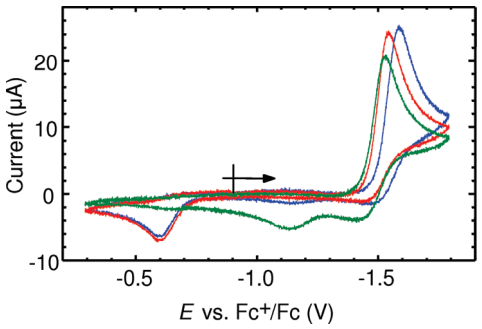

Figure 5. Background-corrected voltammograms of 1.01 mM **3** (blue), 1.00 mM **4** (red), and 1.00 mM **5** (green) in acetonitrile with 0.10 M tetrabutylammonium hexafluorophosphate at glassy carbon (0.10 V/s; scan segments: −0.9 to −1.8 V; −1.8 to −0.3 V; −0.3 to −0.9 V; argon purged).

A primary one-electron reduction with a peak potential around −1.55 V is observed followed by a less distinct second reduction feature at least a further 600 mV more negative. The conclusion that the reduction peak corresponds to a one-electron process is based on comparison of the peak height with that of other known one-electron processes, such as the oxidation of ferrocene, measured under the same conditions. For information about the electronic structure of the one-electron reduction product, see section "Electronic Structure and Observed Properties" below. Strong irreversible oxidation peaks are seen between 0.70 and 0.80 V. Small oxidation peaks are observed for compounds **3** and **4** at −0.60 V but only following an initial scan through the primary reduction peak (see SI-1 and SI-4), suggesting that this feature is due to the oxidation of a species formed upon reduction of the initial compound (this feature is largest at slow scan rates, suggesting that it is due to a species formed in a slow reaction following the initial reduction, SI-2 and SI-5). All three compounds have a degree of chemical reversibility to the primary reduction feature at the larger scan rates (see SI-2, SI-5, and SI-8). At 0.1 V/s, as in Figures 4 and 5, only the Te compound, **5**, shows distinct reversibility. There is a small positive shift, ∼70 mV, in the primary reduction peak potential as S is changed to Se and to Te (from Figure 5: $E_{p,red}$ = −1.602 V (**3**), −1.551 V (**4**), and −1.535 V (**5**)). The second more negative reduction peak is chemically irreversible for all three compounds. The anodic peak potentials span a range of ∼100 mV, with the Te compound being the most easily oxidized and S most difficult (from Figure 4: $E_{p,ox}$ = 0.810 V (**3**), 0.778 V (**4**), and 0.708 V (**5**)). The finding that the Te compound, **5**, is both the easiest to reduce and the easiest to oxidize is surprising, although the magnitudes of the shifts are fairly small. The oxidation peak is chemically irreversible for all three compounds.

Catalysis of the reduction of weak acids by compounds **3**−**5** was tested with additions of acetic acid to acetonitrile solutions (see Figures 6, 7, SI-3, SI-6, SI-9, and SI-10). The response with a 5-fold excess of acid shows some catalysis, indicated by enhanced current in a region where neither the catalyst nor the acid alone are reduced.[58] There is evidence of modest catalysis in this region, most strongly for **3**, with enhanced current around −2.0 V. The feature is broad and not well-defined, so that determination of the overpotential is imprecise but can be considered to be at least 0.5 V (using the standard potential for reduction of acetic acid, −1.46 V).[74] There is little enhancement for **5**, where most of the extra current with 5 mM acid is likely due to the direct reduction of acetic acid on glassy carbon. Compound **4** (Se) represents a case intermediate between compounds **3** (S) and **5** (Te). Figure 7 shows the response with a much larger acid excess, 50:1, wherein any catalytic current is mostly swamped by direct reduction. The addition of acetic acid to these compounds does not lead to growth in the height of the primary reduction peak; such growth was not expected, as this would represent an extremely low overpotential of ∼0.10 V. due to the direct reduction of acetic acid on glassy carbon. Compound **4** (Se) represents a case intermediate between compounds **3** (S) and **5** (Te). Figure 7 shows the response with a much larger acid excess, 50:1, wherein any catalytic current is mostly swamped by direct reduction.

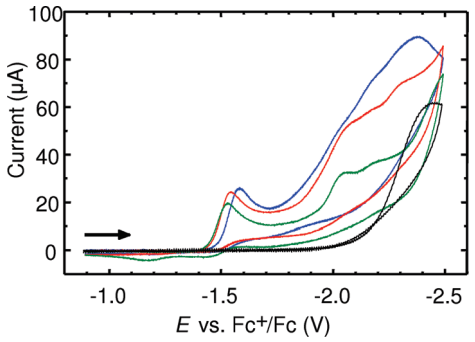

Figure 6. Background-corrected voltammograms of 1.01 mM **3** + 5 mM acetic acid (blue), 1.00 mM **4** + 5 mM acetic acid (red), 1.00 mM **5** + 5 mM acetic acid (green), and 5 mM acetic acid only (black) in acetonitrile with 0.10 M tetrabutylammonium hexafluorophosphate at glassy carbon (0.10 V/s, argon purged); scan: −0.9 to −2.5 V and return to −0.9 V.

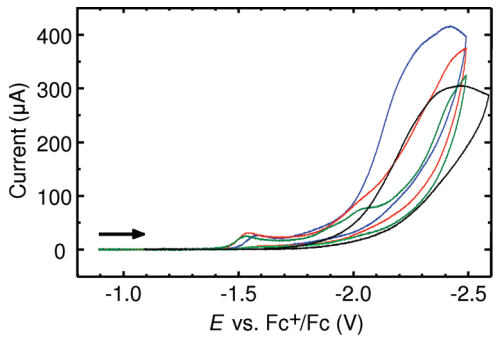

Figure 7. Background-corrected voltammograms of 1.01 mM **3** + 50 mM acetic acid (blue), 1.00 mM **4** + 50 mM acetic acid (red), 1.00 mM **5** + 50 mM acetic acid (green), and 50 mM acetic acid only (black) in acetonitrile with 0.10 M tetrabutylammonium hexafluorophosphate at glassy carbon (0.10 V/s, argon purged); scan: −0.9 to −2.5 V and return to −0.9 V.

Photoelectron Spectroscopy. The He I and He II gas-phase ultraviolet photoelectron spectra of the molecules containing chalcogens S through Te are shown in Figure 8. The general assignment of the ionizations is based on previously reported analogous compounds.[44] The displayed spectrum contains ionizations from the Fe-based metal 3d-orbitals,

(74) Felton, G. A. N.; Glass, R. S.; Lichtenberger, D. L.; Evans, D. H. *Inorg. Chem.* **2006**, *45*, 9181. Corrections: Felton, G. A. N.; Glass, R. S.; Lichtenberger, D. L.; Evans, D. H. *Inorg. Chem.* **2007**, *46*, 5126. Felton, G. A. N.; Glass, R. S.; Lichtenberger, D. L.; Evans, D. H. *Inorg. Chem.* **2007**, *46*, 8098.

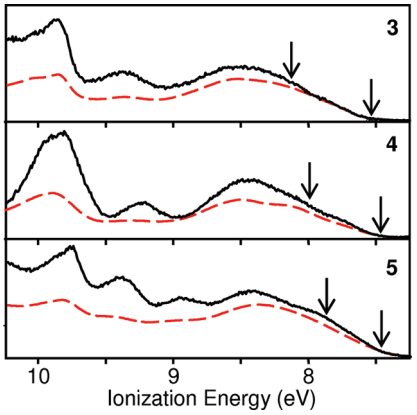

Figure 8. He I (black solid line) and He II (red dashed line) photoelectron spectra of oxetane molecules. The arrows around 7.5 eV indicate the DFT-calculated adiabatic ionization energy for each molecule. The arrows around 8 eV indicate the DFT-calculated vertical ionization energy for each molecule.

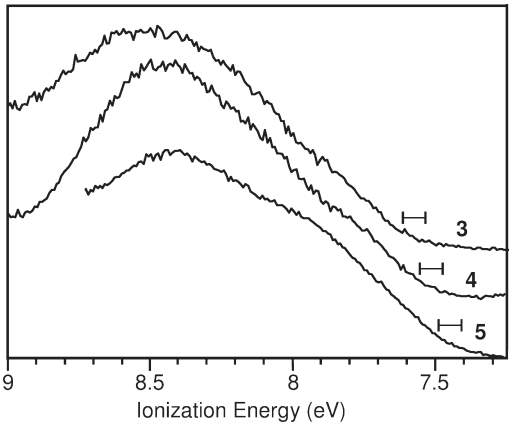

Figure 9. First ionization bands of molecules **3**−**5** in the He I photoelectron spectra. The brackets indicate the region of onset of ionization intensity, which approximates the adiabatic ionization energy for the molecules.

chalcogen-based valence p-orbitals, and O-based 2p-orbitals. The metal d-based ionizations include a formal metal−metal bond of the diiron center and the three occupied d-orbitals of each Fe center that are involved in back-bonding to the carbonyl ligands. The chalcogen-based and O-based valence p-orbital ionizations are expected to be observed in the high ionization energy side of this region based on previously reported photoelectron spectra of chalcogen-[75−77] and oxetane-[78,79]containing organometallic compounds.

The first broad ionization profile, shown in more detail in Figure 9, contains the predominantly Fe d-based ionizations and ranges up to about 9 eV for the S- and Se-containing molecules and up to about 8.7 eV for the Te-containing molecule. This band has a weak shoulder on the low ionization energy side corresponding to ionization from the HOMO of the molecule, calculated to be predominantly the Fe−Fe σ-bond (vide infra), with an adiabatic ionization energy approximately in the region indicated by the onset of ionization intensity around 7.5 eV. The estimated shift of the adiabatic ionization energy from molecule **3** to molecule **5** based on these spectra is 0.1 eV, which is the same as the observed shift in oxidation potentials reported above.

The second and third distinct ionization bands (shown in Figure 8), ranging from about 9.0 to 9.5 eV, are chalcogen based, and above 10.0 eV are O p-based ionizations. The additional identifiable band in this region of the spectrum of **5** is most likely the consequence of spin−orbit effects for the heavy tellurium atom. Compared to the ionizations observed in the He I spectra, these chalcogen-based ionizations exhibit substantially decreased intensity relative to the Fe d-based ionizations when the higher-energy He II excitation was used. The probability of ionization from a chalcogen p-orbital falls by an average factor of 10 from He I to He II excitation, while the probability of O p-orbital and Fe d-orbital ionizations increases by almost a factor of 2 based on theoretical partial photoionization cross-sections of the atoms.[80] However, the relative intensity changes observed in the photoelectron spectra are much less in magnitude than the theoretical values predicted for pure atomic orbital ionizations. This suggests substantial mixing of chalcogen character with iron d orbital and oxygen p orbital character. The energies of these ionizations visibly decrease with substitution from S to Se to Te, as expected from the decreasing electronegativity of the atoms and the decreasing inherent stability of the atomic orbitals.

Electronic Structure and Observed Properties. Density functional theory calculations of these oxetane compounds have been carried out to provide further information on how the electronic structure and properties of the molecules are altered as the chalcogen is changed from S to Se to Te. A computational methodology has been developed previously for [FeFe]-hydrogenase mimics that shows good agreement between calculated and experimental results.[44,58−60] This is the first test of the computational model to account for the properties of a mimic with tellurium atoms in the bridging positions. Optimized geometries and comparisons with the crystal structures are provided in the Supporting Information. For the S- and Se-containing molecules **3** and **4** the calculated Fe−Fe and Fe−chalcogen bond distances are within 0.025 Å of those obtained from crystal structures (see SI). For the Te-containing molecule **5** the optimized Fe−Fe distance is 0.05 Å shorter than the crystal structure distance, and the Fe−Te distance is about 0.07 Å longer than the crystal structure distance. There was some concern about additional relativistic effects or other limitations of the basis set or model for the heavy tellurium atoms, but this was not found to be an issue for the electron distribution or the spectroscopic and thermodynamic properties of the molecule, as evidenced by agreement with the carbonyl stretching frequencies, molecular ionization energies, and oxidation and reduction potentials. It was noted that geometry optimization was much more difficult for the Te-containing molecule because of a fairly flat potential energy surface, perhaps due to the larger and softer tellurium atoms, leading to larger differences in the calculated distances from

(75) Guillemin, J. C.; Bajor, G.; Riague, E.; Khater, B.; Veszpremi, T. *Organometallics* **2007**, *26*, 2507.
(76) Cozzolino, A. F.; Gruhn, N. E.; Lichtenberger, D. L.; Vargas-Baca, I. *Inorg. Chem.* **2008**, *47*, 6220.
(77) Cranswick, M. A.; Gruhn, N. E.; Oorhles-Steele, O.; Ruddick, K. R.; Burzlaff, N.; Schenk, W. A.; Lichtenberger, D. L. *Inorg. Chim. Acta* **2008**, *361*, 1122.
(78) Roszak, S.; Kaufman, J. J.; Koski, W. S.; Barreto, R. D.; Fehlner, T. P.; Balasubramanian, K. *J. Phys. Chem.* **1992**, *96*, 7226.
(79) Mollere, P. D. *Tetrahedron Lett.* **1973**, *14*, 2791.
(80) Yeh, J. J.; Lindau, I. *At. Data Nucl. Data Tables* **1985**, *32*, 1.

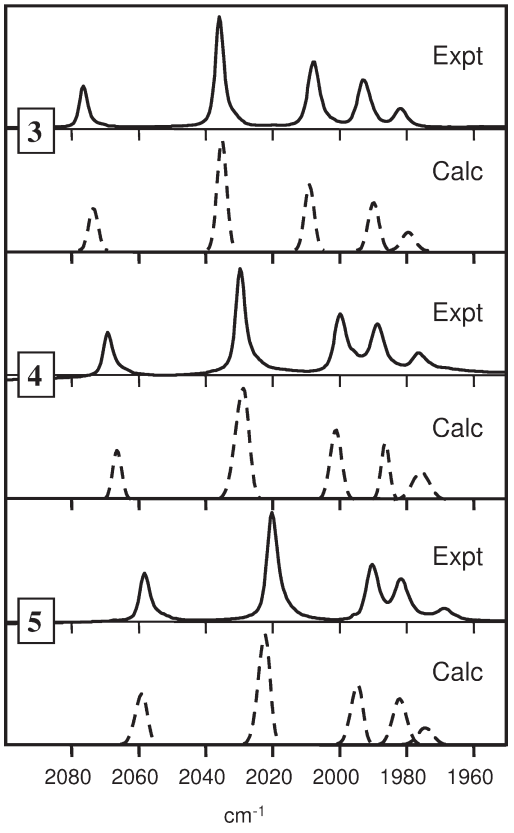

Figure 10. Comparison of the experimental IR spectra (in Nujol) in the carbonyl stretching region (solid lines) with calculated IR spectra (dashed lines) for each of the oxetane molecules.

experiment, but not to significantly larger differences in the calculated energy quantities.

The carbonyl stretching frequencies are an energy measure sensitive to the electron distribution in the molecules, and the intensities of the normal mode absorptions are sensitive to the molecular geometry and carbonyl coupling. The calculated and observed spectra are compared in Figure 10. The average difference in the calculated and experimental frequencies is less that 0.2%, and the relative absorption intensities are in good agreement. As mentioned previously, the decrease in carbonyl stretching frequencies from **3** to **4** to **5** indicates an increase of electron richness at the diiron core of the molecule from S to Se to Te. The trend is as expected considering the changes in electronegativity from S to Se to Te. The increasing donor ability from S to Se to Te is evidenced by the increasing positive charge on these atoms. Based on Voronoi deformation densities, which are less sensitive to basis sets than Mulliken population analysis,[81] the electron density in the vicinity of the chalcogen decreases by 0.06 e^- from S to Se and another 0.09 e^- from Se to Te. Much of the charge is transferred to the carbonyls, and the corresponding increases in electron density in the vicinity of the Fe atoms are 0.02 and 0.04 e^-.

The agreement of the calculations with the experimental ionization energies is also very good. The arrows in Figure 8 indicate the adiabatic and vertical ionization energies as calculated by the Δ*S*CF energy between the neutral molecule and the positive ion. The calculated first vertical ionization energies, for which the structures of the positive ions are constrained to the optimized structures of the neutral molecules, are able to account for the shift of the primary ionization band intensity to lower energy from S to Se to Te substitution. Calculated adiabatic ionization energies, for which the structures of the positive ions are optimized to their global minima, are close to the experimental onset energies of the first ionization bands, indicated by the arrows near 7.5 eV in Figure 8. In each case the global minimum structure of the cation in the gas phase has a semibridging carbonyl ligand, as shown in Figure 11. This general arrangement of the carbonyl ligands, which has been has been the subject of much attention,[59,82−87] has been termed the "rotated" structure because it can be viewed as an approximate 60° rotation of one $Fe(CO)_3$ group. This rotated structure creates a vacant axial coordination site on the Fe center analogous to the active site of [FeFe]-hydrogenase.[19,21,23,88,89]

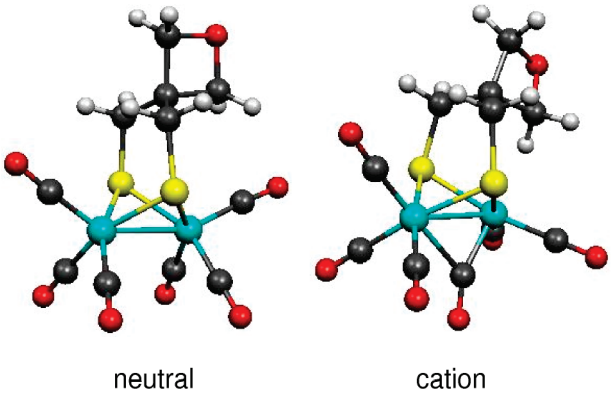

Figure 11. Calculated neutral and cation structures of **3**.

The cation reorganization energy for each molecule was calculated as the energy difference of the optimized semibridged rotated structure of the cation shown in Figure 11 (corresponding to the adiabatic ionization energy) from the energy of the cation calculated with the nonbridged frozen structure of the neutral molecule (corresponding to the vertical ionization energy). Reorganization energies are calculated to be 0.59 eV for **3**, 0.53 eV for **4**, and 0.42 eV for **5**. Substantial reduction of reorganization energy was calculated with increasing atomic radii of the chalcogen, favoring increasing electron transfer rates from S- to Te-containing molecule. The decrease in the reorganization energy was not as great as observed from S to Se in $[\mu$-$Se(CH_2)_2$-$CHCH_3Se][Fe(CO)_3]_2$, where the energies decreased from 0.65 to 0.45 eV.[44] Interestingly, although the vertical ionizations shift significantly to lower energy with the heavier chalcogens, reflecting their greater donor ability, the reorganization energies also decrease down the series, and the

(81) Guerra, C. F.; Handgraaf, J. W.; Baerends, E. J.; Bickelhaupt, F. M. *J. Comput. Chem.* **2004**, *25*, 189.
(82) van der Vlugt, J. I.; Rauchfuss, T. B.; Whaley, C. M.; Wilson, S. R. *J. Am. Chem. Soc.* **2005**, *127*, 16012.
(83) Justice, A. K.; Zampella, G.; DeGioia, L.; Rauchfuss, T. B.; vanderVlugt, J. I.; Wilson, S. R. *Inorg. Chem.* **2007**, *46*, 1655.
(84) Justice, A. K.; Zampella, G.; Gioia, L. D.; Rauchfuss, T. B. *Chem. Commun.* **2007**, 2019.
(85) Justice, A. K.; Rauchfuss, T. B.; Wilson, S. R. *Angew. Chem., Int. Ed.* **2007**, *46*, 6152.
(86) Liu, T.; Darensbourg, M. Y. *J. Am. Chem. Soc.* **2007**, *129*, 7008.
(87) Thomas, C. M.; Darensbourg, M. Y.; Hall, M. B. *J. Inorg. Biochem.* **2007**, *101*, 1752.
(88) Peters, J. W. *Curr. Opin. Struct. Biol.* **1999**, *9*, 670.
(89) Nicolet, Y.; Piras, C.; Legrand, P.; Hatchikian, C.; Fontecilla-Camps, J. C. *Struct. Fold Des.* **1999**, *7*, 13.

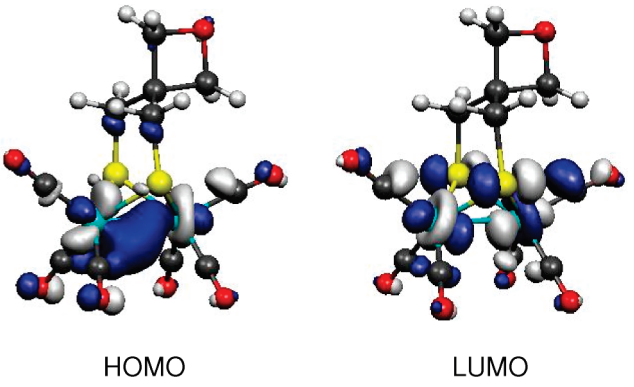

Figure 12. Highest occupied and lowest unoccupied orbitals of **3**.

consequence of the combination of these effects is that there is little shift, only about 0.1 eV overall, in the adiabatic ionization energies, as also seen in the oxidation potentials.

The trend in ionization energies and reorganization energies shows that as the bridging atoms change from S to Se to Te, the cations gain less stabilization in forming the "rotated" structures with the bridging carbonyls. This is counter to the usual expectation that as electron richness at the metal center increases, as shown by the carbonyl stretching frequencies for these molecules, the bridging carbonyl should become more favored because of its greater ability to withdraw and stabilize the electron density. The other important factor in these molecules is that as the chalcogen atoms become larger down the series, there is a corresponding increase in the Fe−Fe distance, such that the bridging carbonyl becomes less effective at favoring the rotated structure. The relative stability of the rotated structure is important to the reduction chemistry and catalysis discussed below.

From plots of the Kohn−Sham orbitals of the HOMO and LUMO, shown in Figure 12, the HOMO is primarily the metal−metal bonding interaction with delocalization of electron density to the carbonyl ligands. The tilt of the oxetane imparts some asymmetry to the HOMO. The LUMO consists mainly of the metal−metal antibonding interaction with some metal−chalcogen antibonding interaction of chalcogen p-orbitals.

The Kohn−Sham orbitals corresponding to the ionizations from 9.0 to 9.5 eV (see SI for orbital plots) were found to contain substantial chalcogen p-orbital character (HOMO−8 to HOMO−10). This is in agreement with the relative intensity of the ionizations observed in He I/He II photoelectron spectra. Also, the orbital (HOMO−11) above 9.5 eV is calculated to contain O 2p character. In addition to the above, mixing of chalcogen orbital characters with Fe and O orbital characters is consistent with the mixing suggested by the He I/He II photoelectron data.

The calculated oxidation and reduction potentials are displayed with the observed cyclic voltammograms in Figure 4. The calculated oxidation potentials that are shown correspond to cation structures without a bridging carbonyl ligand, similar to the neutral molecule. The good agreement between calculated and observed oxidation potentials and their trends suggests that the structures without bridging carbonyl ligands are favored in acetonitrile solution on the time scale of these experiments. Calculated oxidation potentials with a bridging carbonyl ligand in the cation structure gave oxidation potentials in the range 0.51−0.67 V, which agreed less well with experiment, although such structures cannot be ruled out with confidence on this basis.

Various structures also were explored for the anions of these molecules obtained by reduction. For the sulfur-containing molecule **3** the free energy of the structure with the rotated iron center and semibridging carbonyl is calculated to be the same (within 0.01 eV) as the free energy of the structure with the unrotated iron center. For the selenium-containing molecule **4** the free energy of the rotated structure is calculated to be 0.1 eV higher than the unrotated structure, and for the tellurium-containing molecule **5** the difference in free energy between these structures increases again to 0.2 eV. The global minimum structure for the dianions of all three molecules has a bridging carbonyl, along with one broken Fe−chalcogen bond, as found in the study of the corresponding benzenedithiolato[58] and ethanedithiolato[90] complexes. The decreasing favorability of the rotated structures in the anions from S to Se to Te parallels the observed increase in reversibility of the reduction of the Te molecule and the decrease in the rate of reduction of protons to hydrogen observed down this series. Previously, the rate of rotation of the $Fe(CO)_3$ unit has been correlated with the rate of cyanide substitution for carbonyl by an associative mechanism.[28,91] Similarly, these observations strongly indicate that the catalytic reduction of protons by these molecules is promoted by transformation to the rotated structure with the bridging carbonyl to open up the site for protonation and subsequent production of hydrogen.

Conclusion

Diiron dithiolato, diselenolato, and ditellurolato compounds containing an oxetane ring have been prepared in good yields as [FeFe]-hydrogenase models. The oxetane ring remarkably stabilizes the cyclic diselenium and ditellurium precursor compounds, which provides the opportunity to synthesize the homologous S, Se, and Te series **3**−**5**. The objective of this paper was to determine the basis for the difference in reorganization energy of 2Fe2Y (Y = S, Se, and Te) cores. Overall the electronic effects of substitution from S to Se to Te are small. The increasing donor ability of these bridge atoms, as reflected in both the decreasing carbonyl stretching frequencies and the decreasing vertical ionization energies, is compensated by the decreasing reorganization energies such that the adiabatic ionization energies and the electrochemical oxidation potentials occur within narrow energy ranges. The first reduction potentials occur in a similarly small range. However, despite these small changes in potentials, the rate of catalytic reduction of protons to hydrogen is substantially diminished from S to Se to Te. Also diminished is the calculated favorability of the anions to adopt the rotated structures with a bridging carbonyl ligand, which creates an open coordination site on an iron atom for protonation. The increasing size of the chalcogen atoms and the corresponding increasing distance between the iron atoms are likely factors in disfavoring the bridging carbonyl structures.

(90) Felton, G. A. N.; Petro, B. J.; Glass, R. S.; Lichtenberger, D. L.; Evans, D. H. *J. Am. Chem. Soc.* **2009**, *131*, 11290.
(91) Darensbourg, M. Y.; Lyon, E. J.; Zhao, X.; Georgakaki, I. P. *Proc. Natl. Acad. Sci. U.S.A.* **2003**, *100*, 3683.

Acknowledgment. Financial support for this work was provided by the DAAD (Ph.D. grant to M.H.), by the Studienstiftung des Deutschen Volkes (U.-P. Apfel), and by the National Science Foundation through the Collaborative Research in Chemistry program, Grant No. CHE 0527003 (D.H.E., R.S.G., and D.L.L.).

Supporting Information Available: Crystallographic data (excluding structure factors) have been deposited with the Cambridge Crystallographic Data Centre as supplementary publication CCDC-723576 for $Fe_2(\mu\text{-}S_2C_5H_8O)(CO)_6$ (**3**), CCDC-723577 for $Fe_2(\mu\text{-}Se_2C_5H_8O)(CO)_6$ (**4**), and CCDC-723578 for $Fe_2(\mu\text{-}Te_2C_5H_8O)(CO)_6$ (**5**). Copies of the data can be obtained free of charge on application to CCDC, 12 Union Road, Cambridge CB2 1EZ, UK [e-mail: deposit@ccdc.cam.ac.uk]. Supporting Information contains sample input files for calculations, optimized Cartesian coordinates and total energies for all structures, pictures of molecular structures and frontier orbitals, comparison of experimental and calculated geometries, calculated oxidation and reduction potentials, and CV diagrams. This material is available free of charge via the Internet at http://pubs.acs.org.